



## Investigating the role of transportation models in epidemiologic studies of traffic related air pollution and health effects



Maryam Shekarrizfard <sup>a,1</sup>, Marie-France Valois <sup>c,2</sup>, Mark S. Goldberg <sup>c,2</sup>, Dan Crouse <sup>d</sup>, Nancy Ross <sup>e,3</sup>, Marie-Elise Parent <sup>f,4</sup>, Shamsunnahar Yasmin <sup>b,1</sup>, Marianne Hatzopoulou <sup>g,\*</sup>

<sup>a</sup> Department of Civil Engineering and Applied Mechanics, McGill University, 817 Sherbrooke St. W., Room 492, Montréal, Québec, Canada H3A 2K6

<sup>b</sup> Department of Civil Engineering & Applied Mechanics, McGill University, Suite 483, 817 Sherbrooke St. W., Montréal, Québec, Canada H3A 2K6

<sup>c</sup> Department of Medicine, McGill University, Division of Clinical Epidemiology, McGill University Health Centre, QC, Canada H3A 1A1

<sup>d</sup> Department of Sociology, University of New Brunswick, Fredericton, New Brunswick, Canada

<sup>e</sup> Department of Geography, McGill University, 805 Sherbrooke St. W., Montreal, Quebec, Canada H3A 2K6

<sup>f</sup> INRS-Institut Armand-Frappier, Institut national de la recherche scientifique, Unité d'épidémiologie et biostatistique, 531, Boul. des Prairies, Laval, Québec, Canada H7V 1B7

<sup>g</sup> Department of Civil Engineering and Applied Mechanics, McGill University, Macdonald Engineering Building, Room 278b, 817 Sherbrooke St. W., Montréal, Québec, Canada H3A 2K6

### ARTICLE INFO

#### Article history:

Received 19 June 2014

Received in revised form

1 April 2015

Accepted 2 April 2015

#### Keywords:

Traffic-related emissions

Trip-level NO<sub>x</sub> emissions

MOVES

Air pollution

Land-use regression

### ABSTRACT

In two earlier case-control studies conducted in Montreal, nitrogen dioxide (NO<sub>2</sub>), a marker for traffic-related air pollution was found to be associated with the incidence of postmenopausal breast cancer and prostate cancer. These studies relied on a land use regression model (LUR) for NO<sub>2</sub> that is commonly used in epidemiologic studies for deriving estimates of traffic-related air pollution. Here, we investigate the use of a transportation model developed during the summer season to generate a measure of traffic emissions as an alternative to the LUR model. Our traffic model provides estimates of emissions of nitrogen oxides (NO<sub>x</sub>) at the level of individual roads, as does the LUR model. Our main objective was to compare the distribution of the spatial estimates of NO<sub>x</sub> computed from our transportation model to the distribution obtained from the LUR model. A secondary objective was to compare estimates of risk using these two exposure estimates. We observed that the correlation (spearman) between our two measures of exposure (NO<sub>2</sub> and NO<sub>x</sub>) ranged from less than 0.3 to more than 0.9 across Montreal neighborhoods. The most important factor affecting the “agreement” between the two measures in a specific area was found to be the length of roads. Areas affected by a high level of traffic-related air pollution had a far better agreement between the two exposure measures. A comparison of odds ratios (ORs) obtained from NO<sub>2</sub> and NO<sub>x</sub> used in two case-control studies of breast and prostate cancer, showed that the differences between the ORs associated with NO<sub>2</sub> exposure vs NO<sub>x</sub> exposure differed by 5.2–8.8%.

© 2015 Elsevier Inc. All rights reserved.

### 1. Introduction

Traffic-related air pollution has a large impact on public health; in numerous studies associations have been found between

chronic and acute exposures to traffic emissions and respiratory and cardiovascular effects (Cesaroni et al., 2012; Clark et al., 2012; Gan et al., 2011; Janssen et al., 2011; Carlsten et al., 2011; Brook et al., 2010; Jerrett et al., 2009; Marshall et al., 2008; Pope and Dockery 2006). In particular, two recent studies conducted in Montreal, Canada, have shown positive associations between annual estimates of concentrations of nitrogen dioxide (NO<sub>2</sub>), an accepted marker of traffic-related air pollution, and the incidence of postmenopausal breast cancer (Crouse et al., 2010) and of prostate cancer (Parent et al., 2013).

In urban areas, air pollution exhibits substantial seasonal and spatial variability. Different methods have been used to quantify spatial variability, including using data from fixed-site monitoring stations (Brauer and Brook, 1997), land-use regression (LUR) (Johnson et al., 2010; Hoek et al., 2008; Ryan and LeMasters, 2007;

\* Corresponding author. Fax: +1 514 398 7361.

E-mail addresses: [maryam.shekarrizfard@mail.mcgill.ca](mailto:maryam.shekarrizfard@mail.mcgill.ca) (M. Shekarrizfard), [marie-france.valois@mcgill.ca](mailto:marie-france.valois@mcgill.ca) (M.-F. Valois), [mark.goldberg@mcgill.ca](mailto:mark.goldberg@mcgill.ca) (M.S. Goldberg), [dlcrouse@gmail.com](mailto:dlcrouse@gmail.com) (D. Crouse), [nancy.ross@mcgill.ca](mailto:nancy.ross@mcgill.ca) (N. Ross), [marie-elise.parent@iaf.inrs.ca](mailto:marie-elise.parent@iaf.inrs.ca) (M.-E. Parent), [shamsunnahar.yasmin@mail.mcgill.ca](mailto:shamsunnahar.yasmin@mail.mcgill.ca) (S. Yasmin), [marianne.hatzopoulou@mcgill.ca](mailto:marianne.hatzopoulou@mcgill.ca) (M. Hatzopoulou).

<sup>1</sup> Fax: +1 514 398 7361.

<sup>2</sup> Fax: +1 514 843 1493.

<sup>3</sup> Fax: +1 514 398 3747.

<sup>4</sup> Fax: +1 450 686 5599.

Gilbert et al., 2005), and dispersion models (Tartakovsky et al., 2013; Hatzopoulou and Miller, 2010; Beckx et al., 2009; Cook et al., 2008; Dhondt et al., 2012; Lefebvre et al., 2013). LUR models have been developed for many metropolitan areas and are often used to investigate associations between air pollution exposure and specific health effects (Crouse et al., 2009; Arain et al., 2007). However, their reliability in predicting accurate exposures depends on the density of the established monitoring network, which in turn, largely affects the costs of developing a LUR model.

In this paper, we used a transportation model (Sider et al., 2013) with a detailed capability to model emissions from traffic. This transportation model simulates traffic flows and emissions over an entire metropolitan region, and estimates traffic emissions of nitrogen oxides ( $\text{NO}_x$ ) at the level of individual roads. We also make use of a LUR model for nitrogen dioxide ( $\text{NO}_2$ ) developed previously by us for Montreal (Crouse et al., 2009). Finally, we use data from a case-control study of postmenopausal breast cancer and another case-control study of prostate cancer that were previously used to estimate associations with annual traffic-related concentrations of  $\text{NO}_2$  estimated at the residences of all participants (Crouse et al., 2010; Parent et al., 2013). Our main objective was to compare the distribution of the spatial estimates of  $\text{NO}_x$  computed from our transportation model to the distribution of  $\text{NO}_2$  obtained from a LUR model. A secondary objective was to compare estimates of risk using these two exposure estimates; in doing so, we exploited two case-control studies of cancer conducted previously. In fact, an advantage of using emission models to derive exposure relates to their “policy sensitivity”, one could potentially evaluate the effects of changes in land-use, transportation infrastructure, and travel demand on traffic emissions and re-investigate the same associations with health outcomes.

A number of studies have addressed the question of uncertainty in estimating the contribution of traffic to air pollution while others have evaluated the effects of different indices of exposure to traffic-related air pollution (e.g.  $\text{NO}_2$ ,  $\text{NO}_x$ , proximity to traffic, total traffic volume) on health outcomes (Wu et al., 2011; Molitor et al., 2007; Ryan et al., 2007). As an example, Wu et al. (2011) compared different exposure methods: a LUR model, a dispersion model (using the simple Gaussian CALINE4 software), and a traffic-density measure. The authors observed that the risk

of adverse pregnancy outcomes (such as preterm birth) associated with exposure to traffic-related air pollution was smaller when exposures were assigned based on traffic density as compared to LUR or dispersion modeling. Molitor et al. (2007) emphasized the importance of improving exposure assessment through the consideration of advanced techniques in lieu of spatial models such as LUR although no direct comparison between measures was conducted. Their study was mainly focused on the role of spatial autocorrelation in the estimation of health effects.

In this study, our focus is on comparing exposure estimates and evaluating how they may change depending on the model. Our measure of exposure to traffic-generated  $\text{NO}_x$  goes beyond traffic-density (emissions are affected by traffic flows but also by fleet characteristics, speed, and road configuration) and we hypothesize that this measure would be more representative of traffic-related air pollution. Because ambient  $\text{NO}_2$  is largely emitted by vehicular traffic in urban areas, we hypothesize that concentrations of  $\text{NO}_2$  would be associated with emissions of traffic-related  $\text{NO}_x$ . However, because ambient  $\text{NO}_2$  is also affected by other sources (such as industries), we would expect that a model of traffic  $\text{NO}_x$  emissions will underestimate the impact of traffic on  $\text{NO}_2$  away from the roadways. While traffic is not always captured as a predictor in land-use regression models of  $\text{NO}_2$ , the results of LUR may differ from those obtained from transport emission models (Health Effects institute, 2010; Solomon et al., 2012). For example, Crouse et al. (2009) found that the predictive power of their proposed LUR (as measured by the  $R^2$ -squared) was improved by 2–4% after adding traffic data as a predictor.

Our specific objectives were: 1) to generate road-level emissions of  $\text{NO}_x$  in Montreal for summer conditions; 2) to determine the correlation between emissions of  $\text{NO}_x$  with concentrations of  $\text{NO}_2$  derived from a LUR model estimated from sampling in a summer period; and 3) to explore the resulting estimates of risk using these two exposure measures. We only consider the case of comparing “current” estimates of exposure and not of estimating historical ones, although we note that Crouse et al. (2010) have found that the spatial distributions do not vary dramatically over a 10–20 year period. We emphasize that these comparisons in risk are only meant for the purposes of showing a range of plausible estimates between these two methods of estimating exposure to

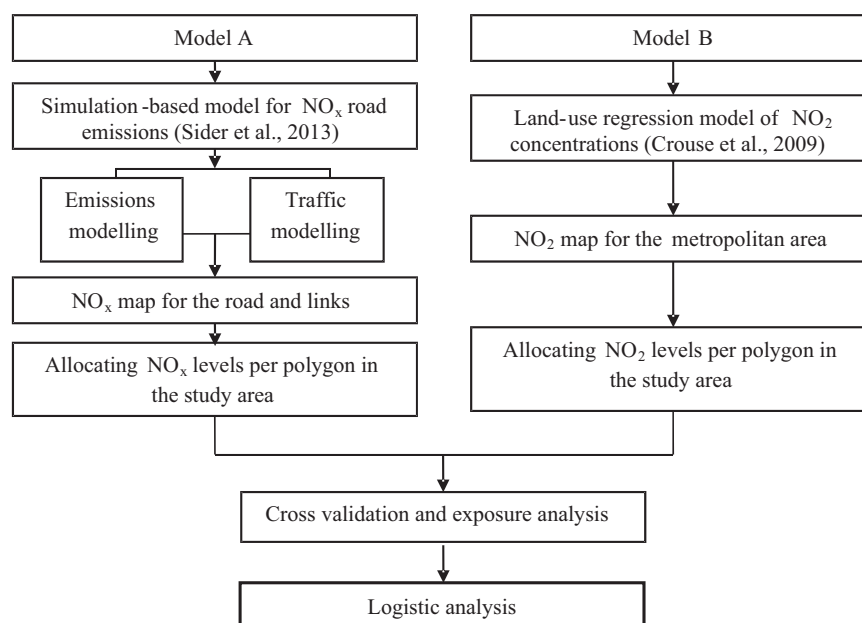


**Fig. 1.** Study methodology including description of data sources (transport model for  $\text{NO}_x$  and LUR for  $\text{NO}_2$ , both reflecting summer conditions), comparing the estimates of  $\text{NO}_x$  and  $\text{NO}_2$ , and estimating odds ratios (OR) for breast and prostate cancer based on the two measures of exposure.

markers of traffic-related air pollution; the risk estimates shown in Crouse et al. (2010) and Parent et al. (2013) derived from an annual LUR model (Crouse et al., 2009) should be considered as the definitive ones.

## 2. Materials and methods

**Fig. 1** presents the study methodology illustrating that we examined the spatial variability of NO<sub>2</sub> concentrations generated from a LUR model for the summer season with NO<sub>x</sub> emissions simulated also for summer conditions across the Island of Montreal. We used both models to generate traffic-related air pollution exposure measures and compared these two measures. **Fig. 2** presents the Island of Montreal where the comparative analysis was undertaken.

### 2.1. Description of data sources

#### 2.1.1. NO<sub>x</sub> emissions

We developed a traffic assignment model for the Montreal region that is linked with an emission model capable of simulating traffic emissions occurring on the road network at the level of each individual driver (Sider et al., 2013). The traffic assignment model (developed in the PTV VISUM platform; PTV Vision, 2009) allocates vehicle flows on the road network using data reflecting the origins and destinations of individual/household trips in an urban area. The model includes road types ranging from expressways to local roads, with details regarding capacity, speed limits, intersection types, and turning restrictions. A dataset of daily travel diaries from the 2008 Origin-Destination (OD) survey was used as input to this model. This survey is conducted every five years in Montreal by the Agence Metropolitaine de transport (AMT, 2008) and contains information on travel behavior for 5% of the Montreal region's households (which can be scaled up to the entire population using sampling weights derived for each geographic sub-area). Our traffic assignment model was validated against traffic counts for the same year at 35 major intersections within the

region as well as five bridges linking the Island of Montreal with the rest of the region. The comparison between actual counts vs. predicted counts provides an  $R^2$  value for the 6–7 a.m. period of 0.78 and a  $R^2$  value for the 7–8 a.m. period of 0.65.

In addition, we developed a vehicle allocation algorithm (Sider et al., 2013) to assign a specific vehicle to each driving trip in the 2008 OD survey (162,364 trips). Working at the household level, the main elements involved with vehicle allocation are the number of vehicles owned by a household, each vehicle's time of availability and geographic coordinates, as well as the vehicle type distribution in the household's neighborhood (which we obtained from the Quebec motor vehicle registry). The database that we obtained from the provincial registry contains information on vehicle age and type. Therefore, every driving trip in the OD survey was allocated a vehicle type and model year that remained constant over a day's worth of trips.

Our output includes traffic flow, average speed, and vehicle mix on every road segment (intersection to intersection) in the region. Using this output, we estimated emissions of nitrogen oxides (NO<sub>x</sub>) at the level of every individual vehicle based on its type, age, speed, and type of road it is circulating on (e.g. highway vs. arterial road with intersections). Emissions were based on a multi-dimensional look-up table of emission factors in grams/vehicle, kilometer that we generated using the Mobile Vehicle Emissions Simulator (MOVES) platform developed by the United States Environmental Protection Agency (USEPA) updated with Montreal-specific data. Individual emission factors that accounted for vehicle type, model year, speed, road type, and season (winter and summer) were generated. In fact, our emission factors were based on hourly temperatures and relative humidity. We also calculated start emissions and these were a function of ambient conditions at the time of starting the vehicle. A total of 4080 EFs were generated.

Total emissions on every roadway segment result from summing the individual emissions of all vehicles on that segment. Because of randomness in the vehicle path choices (traffic assignment) and vehicle type allocation, we ran the model five different times and used averaged emissions for every link. The standard errors associated with the mean emissions are low

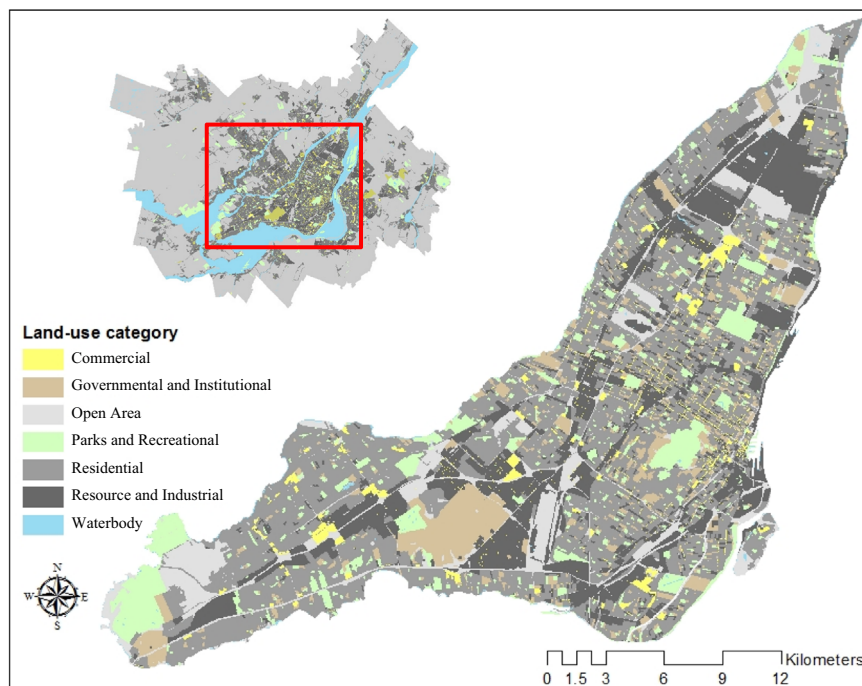


**Fig. 2.** Land use map for the Montreal region featuring the Island of Montreal.

(approximately 1%) indicating that even though allocations may vary drastically at the individual level, segment emissions over the entire day (mean of 24 hourly outputs) remain relatively stable. In this paper, we make use of the  $\text{NO}_x$  emissions derived for summer conditions that represent typical August temperatures and relative humidity.

### 2.1.2. $\text{NO}_2$ concentrations

We made use of estimates of concentrations of  $\text{NO}_2$ , a marker of traffic-related air pollution, from a LUR model that we developed and described previously (Crouse et al., 2009). The model was based on data collected during a series of dense sampling campaigns in 2005 and 2006 to estimate integrated two-week  $\text{NO}_2$  concentrations at individual points in space throughout the entire island. Although we measured concentrations of  $\text{NO}_2$  over a number of periods, in this paper, we are only making use of the August 2006 campaign. During this campaign, two-sided Ogawa passive samplers (Ogawa and Co., USA) were installed at a height of 2.5 m near the sidewalk at 133 locations across Montreal. We then generated a set of variables describing specific land use and road density characteristics measured at different radial distances away from the samplers (100, 300, 500 and 700 m). With these variables, we developed a LUR model to predict concentrations of  $\text{NO}_2$  where measurements were not taken. The resulting model, using concentrations averaged over a two-week sampling period in August, predicted 72% of the variability in  $\text{NO}_2$ . The variables selected for this model included area of commercial land-use, residential land-use, industrial land-use, parks and open water as well as population and building density, length of primary highways and major roads as well as their traffic conditions and distances to shoreline, to National Pollutant Release Inventory Facility (NPRI) and to primary highways. For each  $5 \times 5 \text{ m}^2$  cell, we then used the linear predictor coupled with the land use characteristics of the cell to assign concentrations. The highest concentrations were observed to occur along highways and major urban streets.

### 2.2. $\text{NO}_2$ - $\text{NO}_x$ comparison

Emissions of  $\text{NO}_x$  (summer conditions) derived from the transport model and concentrations of  $\text{NO}_2$  obtained from the LUR model were compared over the entire Island of Montreal (Fig. 2). The concentrations of  $\text{NO}_2$  represent integrated 2-week sampling and the  $\text{NO}_x$  emissions represent a sum of 24-h emissions. Although emissions of  $\text{NO}_x$  on the road network were available for the entire metropolitan region, the LUR model was estimated only

for the Island, therefore restricting our analysis to this geographic area.

While concentrations of  $\text{NO}_2$  were available from a raster-based map at a resolution of  $5 \text{ m} \times 5 \text{ m}$ , emissions of  $\text{NO}_x$  were only derived on the road network. In order to compare the two measures, the Island of Montreal was subdivided into a mesh of grid cells each with dimensions  $80 \text{ m} \times 80 \text{ m}$  amounting to a total of approximately 75,000 grid cells. We allocated to each gridcell a concentration of  $\text{NO}_2$  (in parts per billion, ppb) and a quantity of  $\text{NO}_x$  (in grams). For this purpose, buffers with a radius of 100 m were drawn using the center of every gridcell; the total  $\text{NO}_x$  emissions generated on the roadway and falling within each buffer were summed and allocated to adjacent gridcells. As such, gridcells located in areas with high street density, would receive a larger amount of  $\text{NO}_x$  emissions while gridcells located in regions with low street density would receive little or no emissions.

In contrast,  $\text{NO}_2$  values per gridcell were estimated as the average of the raster values. Different gridcell and buffer sizes were tested and evaluated in terms of how they balanced the following three objectives: 1) minimizing the standard deviation in the  $\text{NO}_2$  values contributing to the average  $\text{NO}_2$  in each gridcell (we observed that  $80 \times 80 \text{ m}^2$  was the largest gridcell size which achieved this objective), 2) maximizing the number of gridcells with non-zero  $\text{NO}_x$  (which led us to create the 100 m buffer that slightly increases the amount of  $\text{NO}_x$  in each gridcell while allowing many gridcells to have a small  $\text{NO}_x$  value rather than a 0), and 3) avoiding a large gap in the  $\text{NO}_2$  and  $\text{NO}_x$  spatial resolutions (if we had generated larger buffer sizes, the  $\text{NO}_2$  and  $\text{NO}_x$  would represent very different areas of influence). Fig. 3 presents the gridcells, buffers, and intersection with road network layer in a small section of Montreal.

We compared the  $\text{NO}_x$  emission load with the concentration of  $\text{NO}_2$  in each gridcell. In addition, we conducted a comparison of the  $\text{NO}_x$  emission load with the measured  $\text{NO}_2$  concentration at each of the 133 passive monitoring stations where ambient  $\text{NO}_2$  was measured in the development of the LUR model as an additional dimension to the validation of our  $\text{NO}_x$  estimates.

We generated scatter plots of  $\text{NO}_x$  vs.  $\text{NO}_2$  and we tested LOESS smoothers with different spans varying from 1% to 75%. To complement the scatter plots and further illustrate the relation between  $\text{NO}_2$  and  $\text{NO}_x$ , we plotted the mean and median  $\text{NO}_x$  within each  $\text{NO}_2$  decile. In addition, we segmented the population of gridcells (and monitoring stations) according to proximity to roadways (using the total length of roads) and examined the correlation between  $\text{NO}_x$  and  $\text{NO}_2$  within each category.

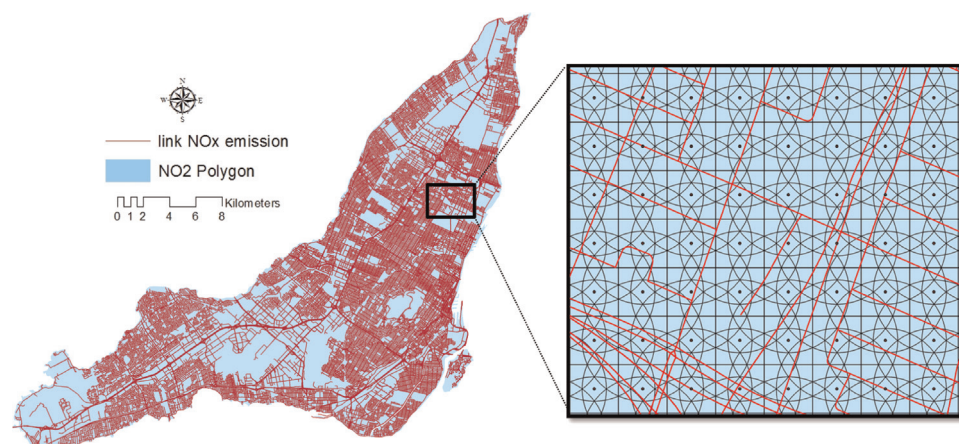


**Fig. 3.** A schematic representation of buffer generation and intersection with roadway segments. Red lines represent the roads. The buffers are drawn around the center of every gridcell. All road segments intersecting a buffer contribute to the  $\text{NO}_x$  emissions allocated to the gridcell. (For interpretation of the references to color in this figure legend, the reader is referred to the web version of this article.)

Finally, in order to map NO<sub>2</sub> and NO<sub>x</sub> values in a way that allowed us to visualize areas with stronger agreement between the two measures, we categorized the 75,000 raw values of NO<sub>x</sub> and NO<sub>2</sub> into deciles and assigned to each gridcell the decile number for NO<sub>2</sub> and for NO<sub>x</sub>. In this respect, scaled NO<sub>x</sub> and NO<sub>2</sub> values ranged from 1 to 10, with 1 indicating the lowest decile. This scaling allowed us to calculate scaled pollutant differences as NO<sub>2</sub> minus NO<sub>x</sub> (ranging from -9 to +9). These scaled differences are referred to as the 'indicator of agreement'. When the difference is 'small' (between -1 and +1), NO<sub>2</sub> and NO<sub>x</sub> values agree while large negative differences indicate a much higher NO<sub>x</sub> value and large positive differences indicate a much higher NO<sub>2</sub> value. Using the scaled difference values for each of the 75,000 polygons, we generated an 'agreement map' highlighting the areas where the two measures agree and areas with high disparities. This type of scaling was only used to visually represent the data; it was not used in subsequent statistical analyses. Finally, we computed the mean and median NO<sub>x</sub> in each NO<sub>2</sub> decile and observed their relationship. In a recent study, Han et al. (2011) observed that the correlation between NO<sub>x</sub> and NO<sub>2</sub> near-roadway is different in the daytime and night-time periods with better correlation during the day indicating that integrated measures would mask these nuances. It is important to note that our transport model provides estimates of hourly NO<sub>x</sub> emissions throughout the day therefore accounting for traffic patterns and diurnal temperature changes.

### 2.3. Deriving exposures and associations with breast cancer and prostate cancer

The estimated spatial emissions of NO<sub>x</sub> and concentrations of NO<sub>2</sub> were linked to the residences of 792 and 1722 participants in the breast cancer and prostate cancer case-control studies, respectively (Crouse et al., 2010; Parent et al., 2013). We first compared exposures for the study participants and regenerated the comparative tests that were described in the previous sections to evaluate whether the same relationships hold for the two samples in the case-control studies.

We then estimated ORs for both cancers using estimates of NO<sub>2</sub> and NO<sub>x</sub> by adopting the same methodology and covariates as the original studies. For this purpose, an unconditional logistic regression model was used to estimate ORs and associated 95% CI. Each exposure measure was included as a continuous linear variable (after verifying this assumption through the use of natural cubic functions of the exposure-response curves). Different sets of covariates were included in the two different cancer studies, and these variables included the cancer-specific set of accepted and suspected risk factors. All risk factors including descriptions of cancer cases and controls are presented as supplementary material. Covariates were included in the analysis in both forms of linear and natural cubic spline functions. We presented ORs for an increase across the interquartile range (IQR) of NO<sub>2</sub> and NO<sub>x</sub>: 2.71 ppb and 481.37 g, respectively. The IQR is defined based on the exposures of subjects (cases and controls).

**Table 1**  
Descriptive statistics for NO<sub>x</sub> and NO<sub>2</sub> across gridcells.

Variable	Minimum	Maximum	Mean	Median	Variance	Percentiles			IQR <sup>a</sup>
						25	50	75	
NO <sub>2</sub> (ppb)	0.00	46.88	7.91	7.56	9.72	6.028	7.56	9.37	3.342
NO <sub>x</sub> (g)	0.00	21589.51	788.84	174.34	4.2e6	28.57	174.35	527.03	498.46

<sup>a</sup> IQR, interquartile range.

## 3. Results and discussion

### 3.1. NO<sub>2</sub>-NO<sub>x</sub> comparison

**Table 1** describes the distribution of concentrations of NO<sub>2</sub> and NO<sub>x</sub> across the 75,000 gridcells; values of NO<sub>2</sub> and NO<sub>x</sub> ranged from 0 to 46.88 ppb and 0 to 21589.51 g respectively. Fig. 4a presents segment-level NO<sub>x</sub> emissions clearly showing that the most emitting facilities are the major highways running across the city as well as main arterial roads. The red and green lines in Fig. 4a represent the segments with the highest and lowest emission levels, respectively. NO<sub>x</sub> emissions were classified using ArcMap based on natural data groups which are located between two consecutive low points (valleys) in a histogram. As a result of this technique, the differences between classes are maximized. Fig. 4b presents the NO<sub>2</sub> raster map generated using the August LUR model for the same geographic area (Crouse et al., 2009). The shades of gray refer to the NO<sub>2</sub> concentrations with the highest concentrations represented in the lightest shade and occurring around the highways and in the downtown area. The scale of the NO<sub>2</sub> LUR map is inverted (highest concentrations in the lightest shades) in order to better visualize the overlay between the NO<sub>2</sub> map and NO<sub>x</sub> emissions on roads presented in Fig. 4c. Qualitatively, we can observe that road segments highlighted in bright red and orange (which represent the highest emitting roads) overlap with the light shaded areas on the NO<sub>2</sub> map.

Using the NO<sub>2</sub> and NO<sub>x</sub> levels for the 75,000 gridcells, we calculated the Spearman correlation coefficient to be 0.28 (95% CI: 0.27–0.29). Fig. 5 presents the scatterplot of NO<sub>2</sub> vs. NO<sub>x</sub> and LOESS smoother with a 1% span illustrating a non-linear relationship between the two measures. The correlation between simulated NO<sub>x</sub> and observed NO<sub>2</sub> at the 133 monitoring stations was also estimated; the Spearman correlation coefficient was 0.45 (95% CI: 0.31–0.58). Fig. 6 presents the scatterplot and LOESS smoother of 15% also illustrating a non-linear relationship.

These same relationships between NO<sub>2</sub> and NO<sub>x</sub> across the 75,000 gridcells and at the 133 stations can also be visualized in Figs. 7 and 8 where the mean and median NO<sub>x</sub> values are plotted within each NO<sub>2</sub> decile. We observed that the fastest increase in mean NO<sub>x</sub> occurs when NO<sub>2</sub> concentrations are in the highest deciles characterizing concentrations near roadways. Indeed, closer to the roadways, NO<sub>x</sub> emissions are highest since NO<sub>x</sub> emissions are estimated only on the roads.

In order to investigate the effect of proximity to a roadway on the relationship between NO<sub>2</sub> and NO<sub>x</sub>, polygons were classified according to the total lengths of roads (in meters) within their buffer. Spearman correlation coefficients were calculated in each category. Fig. 9 shows that the correlation between NO<sub>2</sub> and NO<sub>x</sub> increases significantly with the increase in the density of roads within a polygon. For polygons affected by close to 1400 m of roadways within their buffers, the correlation with NO<sub>2</sub> is 0.85 while at road densities of about 400 m per polygon, the correlation drops to less than 0.3. Fig. 10 illustrates that the same trend is observed when comparing NO<sub>x</sub> with the NO<sub>2</sub> concentrations at the 133 monitoring stations.

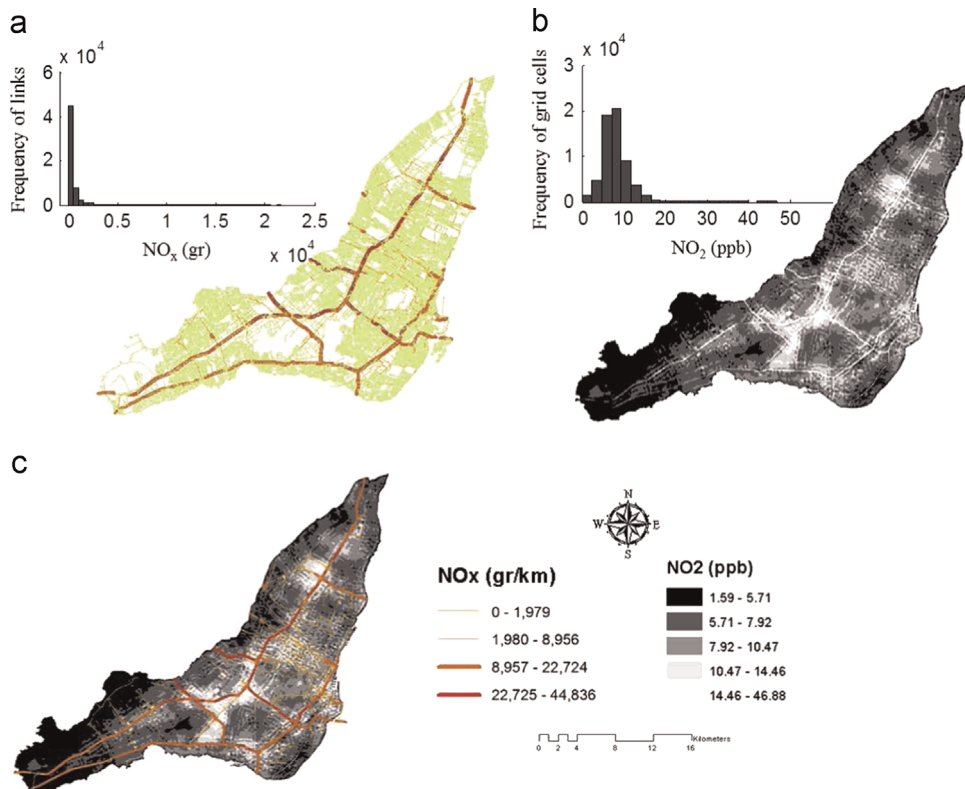


**Fig. 4.** Visualizing NO<sub>x</sub> and NO<sub>2</sub> levels across the Montreal region. (a) Segment emissions presented at four different levels with green segments as the lowest emitting and red segments with the highest emissions; (b) NO<sub>2</sub> August concentrations illustrated at five different levels with dark shades representing the lowest concentrations and light shades the highest concentrations; and (c) overlay of the two maps in a and b to visualize agreement between NO<sub>2</sub> and NO<sub>x</sub>. (For interpretation of the references to color in this figure legend, the reader is referred to the web version of this article.)

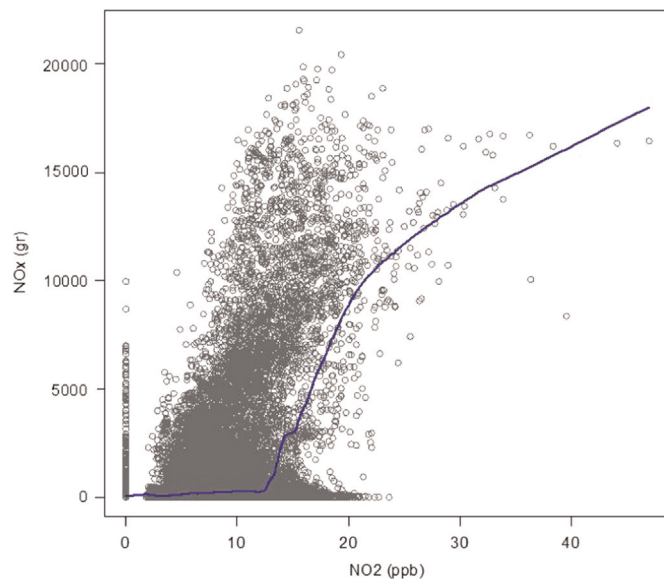


**Fig. 5.** Predicted NO<sub>2</sub> vs. simulated NO<sub>x</sub> across the 75,000 gridcells with LOESS (1% span).

In order to spatially map NO<sub>2</sub> and NO<sub>x</sub> values and using the scaled difference values for each of the 75,000 polygons, we generated an ‘agreement map’ highlighting the areas where the two measures agree and areas with high disparities (Fig. 11). When the difference is close to 0 (between -1 and +1), it indicates a good agreement between both measures. A large positive difference indicates that the NO<sub>2</sub> scaled value is much higher (this is expected to occur in areas with little roadways) while a large

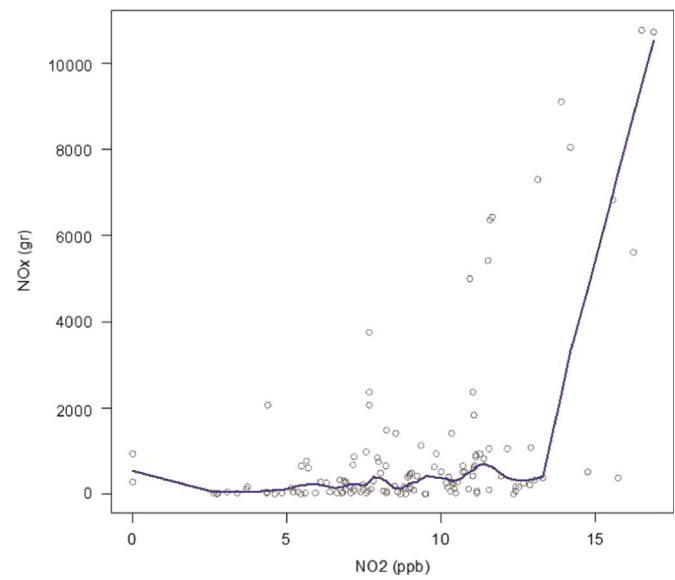


**Fig. 6.** Observed NO<sub>2</sub> vs. simulated NO<sub>x</sub> at the 133 stations with LOESS (15% span).

negative difference indicates that the NO<sub>x</sub> value is larger (this is expected to occur in the vicinity of roadways). Traffic emissions of NO<sub>x</sub> are the precursor to NO<sub>2</sub> in urban areas. Therefore NO<sub>2</sub> is high where NO<sub>x</sub> emissions are high as well. Therefore closer to roadways, we expect that NO<sub>2</sub> and NO<sub>x</sub> values are correlated because the variation in NO<sub>x</sub> (due to a variation in traffic volumes, speeds, and composition) will be followed by a similar variation in NO<sub>2</sub>. Far from the roadways, other sources of NO<sub>2</sub> (albeit small) will become more important. In this situation, we expect that the

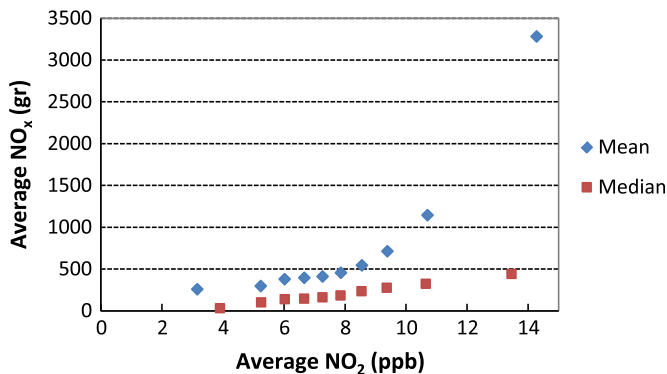


**Fig. 7.** Mean and median NO<sub>x</sub> emissions vs. mean and median NO<sub>2</sub> concentrations in each NO<sub>2</sub> decile (using data from the 75,000 gridcells).

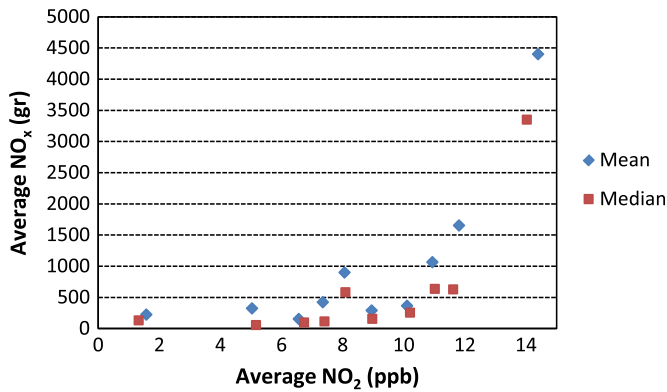


**Fig. 8.** Mean and median NO<sub>x</sub> emissions vs. mean and median NO<sub>2</sub> concentrations in each NO<sub>2</sub> decile (based on NO<sub>2</sub> at the 133 monitoring stations).

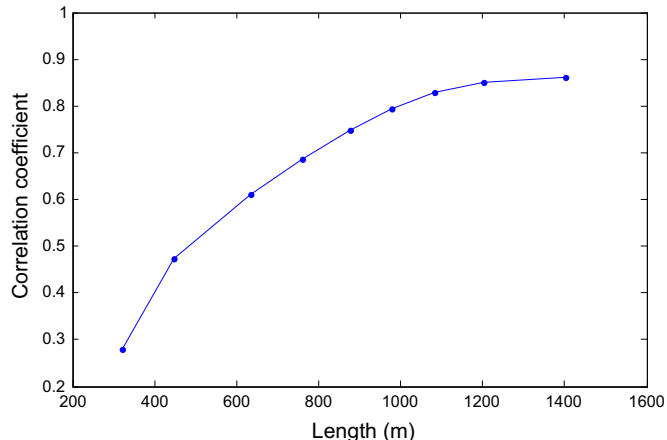


**Fig. 9.** Spearman correlations between NO<sub>x</sub> and NO<sub>2</sub> for different polygon sets classified using the road length in each polygon (using the 75,000 polygons). The correlation coefficients are higher at higher road density.

transport/emission model will underestimate exposure. **Fig. 11a** illustrates the frequency distribution of scaled pollutant differences across the 75,000 polygons. We observed that for 38.9% of polygons, the agreement was between  $-1$  and  $+1$ . Similarly **Fig. 11b** provides a map of the scaled difference for each polygon across the Island of Montreal. It illustrates that the regions with highest agreement are close to the roadways and within the central areas of the city (highly populated) while regions with positive scaled differences are far from roadways and regions with negative scaled differences are very close to some roadways whereby the NO<sub>x</sub> level per polygon would be extremely high. This indicates a potential limitation of the NO<sub>x</sub> model which does not

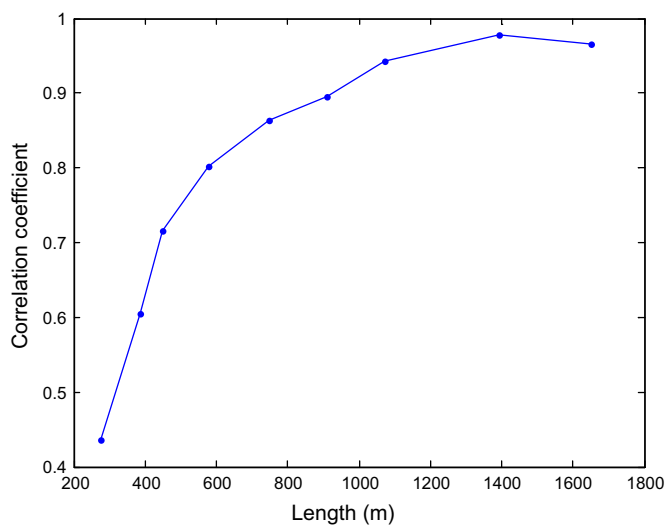


**Fig. 10.** Spearman correlations between NO<sub>x</sub> and NO<sub>2</sub> for different fixed stations classified using the road length in each polygon containing the station (using the 133 stations). The correlation coefficients are higher at higher road density.

include atmospheric dispersion therefore tending towards overestimating the contribution of traffic to air pollution in the vicinity of roads and underestimating air pollution away from roadways (where the contribution of other sources becomes more important).

### 3.2. Differences in risk estimates obtained using the NO<sub>x</sub> model and the summer LUR: examples from two case-control studies

**Fig. 12** illustrates a ‘heat map’ representing the home locations of the 792 breast cancer participants (cases and controls) overlaying our ‘agreement map’. We observed that 34% of the participants lived in areas with scaled differences between both measures of  $-1$ ,  $0$ , and  $+1$  (indicating ‘reasonable agreement’) and 0.86% lived in areas where the scaled differences are  $-8$  and  $-9$  indicating close proximity to roadways. **Fig. 13** shows that for 50% of the participants, the Spearman correlation between NO<sub>x</sub> and NO<sub>2</sub> is 0.5 or higher (up to 0.9). Comparing this figure with **Fig. 9** that presented the correlations for the entire domain based on road length; we found that the road length in the buffers where breast cancer subjects reside was higher. Similar results were found for subjects from the prostate cancer study (data not shown).

We estimated separate ORs using concentrations of NO<sub>2</sub> and emissions of NO<sub>x</sub> as measures of exposure, both for the breast cancer and prostate cancer case-control studies. In total, 792 individuals were included in the breast cancer study and 1772 subjects were included in the prostate cancer analysis (including both cases and controls). **Table 2** shows that the odds ratios estimated using the two exposure metrics differed between 5.2% and 8.8%, suggesting that either method for estimating traffic-related pollution would produce similar estimates of risk.

We reiterate that the purpose of this analysis is not to show whether there is an association for these limited exposure data, as we have already published on these using the land use regression models (Crouse et al., 2010; Parent et al., 2013), but rather whether the estimates of risk are similar between the two types of exposure measures.

### 4. Conclusions

Land use regression (LUR) techniques are generally used for deriving exposure levels in epidemiologic studies of air pollution

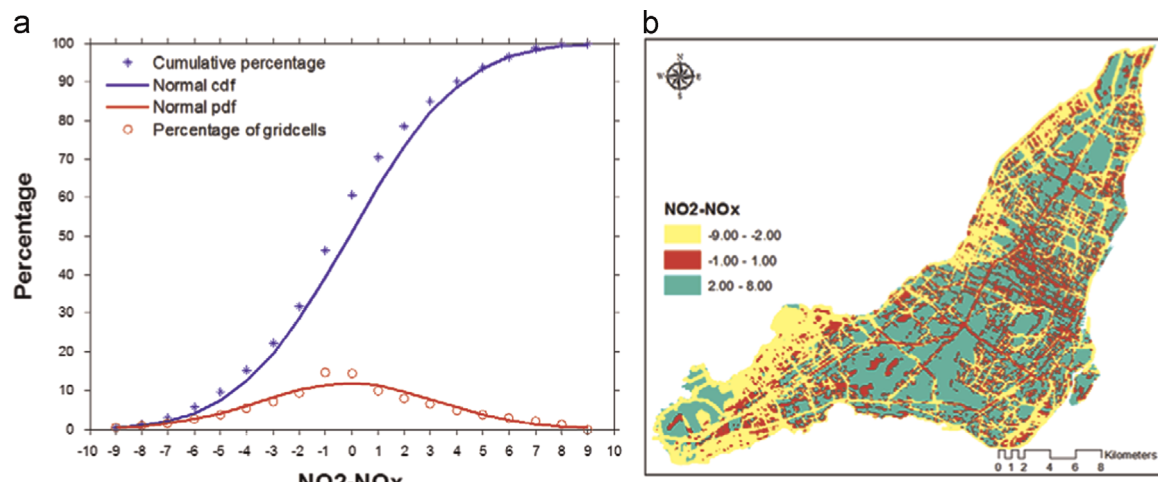


**Fig. 11.** (a) Frequency distribution (cdf: cumulative distribution function and pdf: probability density function) and spatial distribution (b) of scaled pollutant differences (or ‘indicator of agreement’). The red areas indicate a good agreement between both measures occurring in the vicinity of roadways. The green areas indicate that the NO<sub>2</sub> scaled value is much higher. A large negative difference between the scaled values of NO<sub>2</sub> minus NO<sub>x</sub> is presented in yellow. (For interpretation of the references to color in this figure legend, the reader is referred to the web version of this article.)

and health effects. However, they often necessitate the deployment of large air quality sampling campaigns with extensive spatial and temporal coverage. In this paper, we compared a measure of exposure to traffic-related air pollution generated by a transportation model with NO<sub>2</sub> concentrations derived from LUR. We compared the measures of NO<sub>2</sub> and NO<sub>x</sub> across the Montreal Island as well as included a comparison of health risks associated with these exposures.

Our results indicate reasonable agreement between the two models in terms of the spatial distribution of emissions and air quality. In addition, we observe that the two measures lead to similar ORs for breast and prostate cancers. While this study compares modeled concentrations of NO<sub>2</sub> (ppb) to modeled emissions of NO<sub>x</sub> (grams) a number of studies have used modeled

concentrations of NO<sub>2</sub> and NO<sub>x</sub> at participants’ home locations to compare risk estimates. Using LUR-modeled NO<sub>2</sub>/NO<sub>x</sub> concentrations and NO<sub>x</sub> derived from a simple Gaussian dispersion model, Wu et al. (2011) found that the differences in the ORs for preterm birth based on LUR output and dispersion model output vary between 50% and 77% (with the dispersion model output leading to more attenuated ORs); an order of magnitude higher than the difference we observed in this study. Andersen et al. (2011) used a Cox proportional hazard model for obstructive pulmonary disease in Denmark. In the fully adjusted model for age, smoking status, duration, intensity, and environmental tobacco smoke, the authors observed an OR of 1.08 (95% CI: 1.02–1.14) with a 35-year average exposure to measured NO<sub>2</sub> levels and 1.05 (95% CI: 1.01–1.10) with a 35-year average exposure to measured NO<sub>x</sub> levels. In a study by

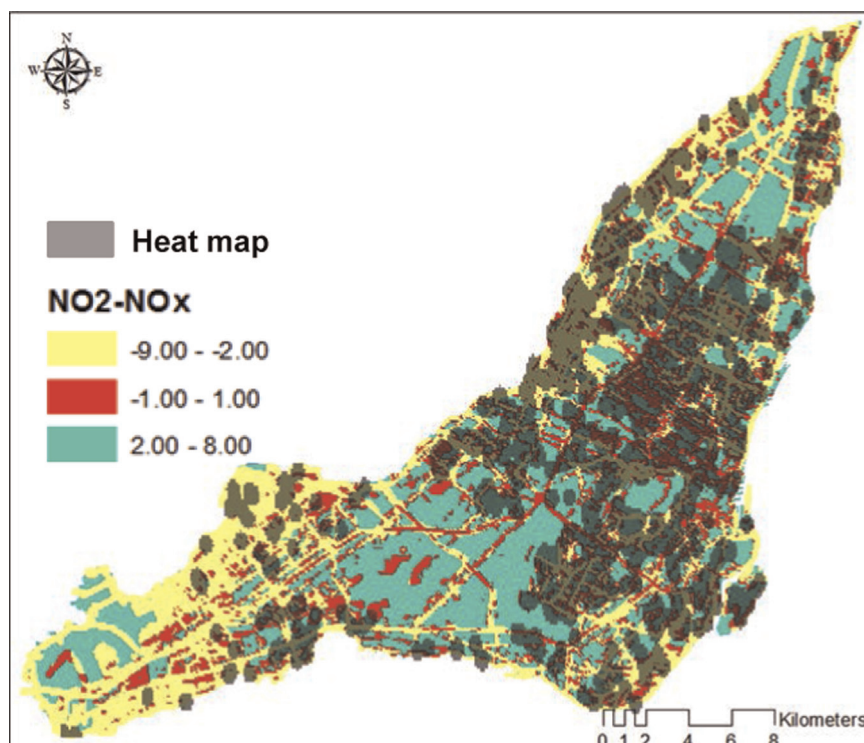


**Fig. 12.** Distribution of sample of breast cancer subjects based on home location.

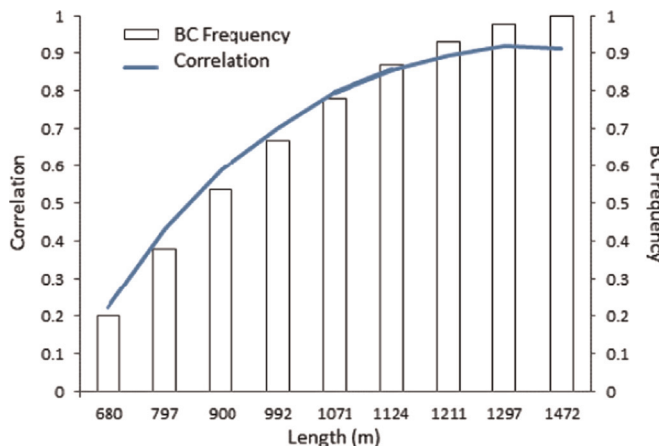


**Fig. 13.** Frequency of breast cancer subjects (represented as BC frequency) and spearman correlation between  $\text{NO}_x$  and  $\text{NO}_2$  for areas with different road lengths. The continuous blue line presents the correlation coefficient. This figure shows that the correlation between  $\text{NO}_x$  and  $\text{NO}_2$  and the frequency of BC subjects increase with the increase in the density of roads within a polygon. (For interpretation of the references to color in this figure legend, the reader is referred to the web version of this article.)

**Table 2**

Odds ratios for breast and prostate cancer for pollutants modeled as linear effects for a change equivalent to the IQR, age-adjusted and fully-adjusted models.

Model and exposure measure	For increase of IQR <sup>a</sup> for OR and 95% CI	
	OR	95% CI for OR
Breast cancer	Age adjusted <sup>b</sup>	
	August $\text{NO}_2$	1.09
	Summer $\text{NO}_x$	1.04
	Percent difference in ORs	5.5%
	Fully adjusted	
	August $\text{NO}_2$	1.14
	Summer $\text{NO}_x$	1.04
	Percent difference in ORs	8.8%
Prostate cancer	Age adjusted <sup>b</sup>	
	August $\text{NO}_2$	1.08
	Summer $\text{NO}_x$	1.02
	Percent difference in ORs	5.5%
	Fully adjusted	
	August $\text{NO}_2$	0.97
	Summer $\text{NO}_x$	1.02
	Percent difference in ORs	5.2%

<sup>a</sup> The IQR for breast cancer is 2.706 ppb for the August  $\text{NO}_2$  and 481.376 g for summer  $\text{NO}_x$ . The IQR for prostate cancer is 2.76 ppb for the August  $\text{NO}_2$  and 419.16 g for summer  $\text{NO}_x$ .

<sup>b</sup> Age is modeled as a linear effect.

Chen et al. (2007) on the relation between lung cancer and measured  $\text{NO}_x$  vs.  $\text{NO}_2$  concentrations, the authors found that among trends of different air pollutants (including  $\text{NO}_x$ ,  $\text{PM}_{10}$ , VOC,  $\text{SO}_2$ , Lead), the one with a pattern most similar to the trend in lung cancer incidence was  $\text{NO}_x$ .

The analysis we presented in this study sheds light on the use of two different measures of exposure to traffic-related air pollution. Our two measures are not perfectly correlated; while  $\text{NO}_x$  emissions from traffic are highly correlated with near-road  $\text{NO}_2$  levels, in the absence of a dispersion model, we could be over or underestimating the exposure to  $\text{NO}_x$  emissions away from the roadways. Similarly, LUR techniques are associated with a number of uncertainties and highly depend on the diversity and density of

sampling locations. The differences in the ORs for breast and prostate cancers using both measures are small.

## Information on funding sources supporting the work

This study was funded by a collaborative grant from the Canadian Institutes of Health Research and the Natural Sciences and Engineering Research Council of Canada.

## Funding sources for the cancer studies

The breast and prostate cancer studies were supported financially through grants from the Canadian Cancer Society, the Cancer Research Society, the Fonds de Recherche du Québec—Santé (FRQS), FRQS-RRSE, and the Ministère du Développement économique, de l'Innovation et de l'Exportation du Québec. Marie-Élise Parent has held career awards from the FRQS.

## Appendix A. Supplementary material

Supplementary data associated with this article can be found in the online version at <http://dx.doi.org/10.1016/j.envres.2015.04.002>.

## References

- AMT, Agence Metropolitaine de Transport (AMT), 2008. La mobilité des personnes dans la région de Montréal: Faits Saillants. Enquête Origine-Destination.
- Andersen, Z.J., Hvidberg, M., Jensen, S.S., Ketzell, M., Loft, S., Sorensen, M., et al., 2011. Chronic obstructive pulmonary disease and long-term exposure to traffic-related air pollution: a cohort study. *Am. J. Respir. Crit. Care Med.* 183, 455–461.
- Arain, M.A., Blair, R., Finkelstein, N., Brook, J.R., Sahsuvaroglu, T., Beckerman, B., et al., 2007. The use of wind fields in a land use regression model to predict air pollution concentrations for health exposure studies. *Atmos. Environ.* 41 (16), 3453–3464.
- Beckx, C., Int Panis, L., Arentze, T., Janssens, D., Torfs, R., Broekx, S., et al., 2009. A dynamic activity-based population modelling approach to evaluate exposure to air pollution: methods and application to a dutch urban area. *Environ. Impact Assess. Rev.* 29, 179–185.
- Brauer, M., Brook, J.R., 1997. Ozone personal exposures and health effects for selected groups residing in the Fraser valley. *Atmos. Environ.* 31 (14), 2113–2121.
- Brook, R.D., Rajagopalan, S., Pope III, C.A., Brook, J.R., Bhatnagar, A., Diez-Roux, A.V., et al., 2010. Particulate matter air pollution and cardiovascular disease: an update to the scientific statement from the American Heart Association. *Circulation* 121, 2331–2378.
- Carlsten, C., Dybuncio, A., Becker, A., Chan-Yeung, M., Brauer, M., 2011. Traffic-related air pollution and incident asthma in a high-risk birth cohort. *Occup. Environ. Med.* 68, 291–295.
- Cesaroni, G., Boogaard, H., Jonkers, S., et al., 2012. Health benefits of traffic-related air pollution reduction in different socioeconomic groups: the effect of low-emission zoning in Rome. *Occup. Environ. Med.* 69, 133–139.
- Chen, F., Cole, P., Bina, W.F., 2007. Time trend and geographic patterns of lung adenocarcinoma in the United States, 1973–2002. *Cancer Epidemiol. Biomark. Prev.* 16 (12), 2724–2729.
- Clark, C., Crombie, R., Head, J., van Kamp, I., van Kempen, E., Stansfeld, S.A., 2012. Does traffic-related air pollution explain associations of aircraft and road traffic noise exposure on children's health and cognition? A secondary analysis of the United Kingdom sample from the RANCH project. *Am. J. Epidemiol.* 176, 327–337.
- Cook, R., Isakov, V., Touma, J.S., Benjey, W., Thurman, J., Kinnee, E., et al., 2008. Resolving local-scale emissions for modeling air quality near roadways. *Air Waste Manag. Assoc.* 58, 451–461.
- Crouse, D.L., Goldberg, M.S., Ross, N.A., Chen, H., Labrèche, F., 2010. Postmenopausal breast cancer is associated with exposure to traffic-related air pollution in Montreal, Canada: a case-control study. *Environ. Health Perspect.* 118 (11), 1578–1583.
- Crouse, D.L., Goldberg, M.S., Ross, N.A., 2009. Prediction-based approach to modeling temporal and spatial variability of traffic-related air pollution in Montreal, Canada. *Atmos. Environ.* 43 (32), 5075–5084.
- Dhondt, S., Beckx, C., Degraeuwe, B., Lefebvre, W., Kochan, B., Bellemans, T., et al., 2012. Health impact assessment of air pollution using a dynamic exposure profile: implications for exposure and health impact estimates. *Environ. Impact Assess. Rev.* 32, 1–10.

- Assess. Rev. 36, 42–51.
- Gan, W.Q., Koeoorn, M., Davies, H.W., Demers, P.A., Tamburic, L., Brauer, M., 2011. Long-term exposure to traffic-related air pollution and the risk of coronary heart disease hospitalization and mortality. *Environ. Health Perspect.* 119, 501–507.
- Gilbert, N.L., Goldberg, M.S., Beckerman, B., Brook, J.R., Jerrett, M., 2005. Assessing spatial variability of ambient nitrogen dioxide in Montreal, Canada, with a land-use regression model. *J. Air Waste Manag.* 55, 1059–1063.
- Han, S., Hai, B., Yinchang, F., Aixia, L., Xiangjin, L., Fang, Z., et al., 2011. Analysis of the relationship between O<sub>3</sub>, NO and NO<sub>2</sub> in Tianjin, China. *Aerosol Air Qual. Res.* 11, 128–139.
- Hatzopoulou, M., Miller, E.J., 2010. Linking an activity-based travel demand model with traffic emission and dispersion models: transport's contribution to air pollution in Toronto. *Transp. Res. D: Transp. Environ.* 15 (6), 315–325.
- Health Effects Institute, 2010. Traffic-Related Air Pollution: A Critical Review of the Literature on Emissions, Exposure, and Health Effects. Health Effects Institute, Boston, MA.
- Hoek, G., Beelen, R., De Hoogh, K., Vienneau, D., Gulliver, J., Fischer, P., et al., 2008. A review of land-use regression models to assess spatial variation of outdoor air pollution. *Atmos. Environ.* 42, 7561–7578.
- Janssen, N.A.H., Hoek, G., Simic-Lawson, M., Fischer, P., van Bree, L., ten Brink, H., et al., 2011. Black carbon as an additional indicator of the adverse health effects of airborne particles compared with PM10 and PM2.5. *Environ. Health Perspect.* 119, 1691–1699.
- Jerrett, M., Finkelstein, M.M., Brook, J.R., Arain, M.A., Kanaroglou, P., Stieb, D.M., et al., 2009. A cohort study of traffic-related air pollution and mortality in Toronto, Ontario, Canada. *Environ. Health Perspect.* 117, 772–777.
- Johnson, M., Isakov, V., Touma, J.S., Mukerjee, S., Özkanak, H., 2010. Evaluation of land-use regression models used to predict air quality concentrations in an urban area. *Atmos. Environ.* 44, 3660–3668.
- Lefebvre, W., Degrawe, B., Beckx, C., Vanhulsel, M., Kochan, B., Bellemans, T., et al., 2013. Presentation and evaluation of an integrated model chain to respond to traffic-and health-related policy questions. *Environ. Model. Softw.* 40, 160–170.
- Marshall, J.D., Nethery, E., Brauer, M., 2008. Within-urban variability in ambient air pollution: comparison of estimation methods. *Atmos. Environ.* 42, 1359–1369.
- Molitor, J., Jerrett, M., Chang, C.-C., Molitor, N.-T., Gauderman, J., Berhane, K., et al., 2007. Assessing uncertainty in spatial exposure models for air pollution health effects assessment. *Environ. Health Perspect.*, 1147–1153.
- Parent, M.E., Goldberg, M.S., Crouse, D.L., Ross, N.A., Chen, H., Valois, M.F., Liautaud, A., 2013. Traffic-related air pollution and prostate cancer risk: a case-control study in Montreal, Canada. *Occup. Environ. Med.* 70 (7), 511–518.
- Pope, C.A., Dockery, D.W., 2006. Health effects of fine particulate air pollution: lines that connect. *J. Air Waste Manag. Assoc.*, 709–742.
- PTV Vision, 2009. VISUM 11.0 Basics, PTV AG. PTV Vision, Karlsruhe, Germany.
- Ryan, P.H., LeMasters, G.K., 2007. A review of land-use regression models for characterizing intraurban air pollution exposure. *Inhal. Toxicol.* 19 (s1), 127–133.
- Ryan, P.H., LeMasters, G.K., Biswas, P., Levin, L., Hu, S., Lindsey, M., et al., 2007b. A comparison of proximity and land use regression traffic exposure models and wheezing in infants. *Environ. Health Perspect.* 115, 278–284.
- Sider, T., Alam, A., Zukari, M., Dugum, H., Goldstein, N., Eluru, N., Hatzopoulou, M., 2013. Land-use and socio-economics as determinants of traffic emissions and individual exposure to air pollution. *J. Transp. Geogr.* 33, 230–239.
- Solomon, P.A., Costantini, M., Grahame, T.J., Gerlofs-Nijland, M.E., Cassee, F.R., Russell, A.G., et al., 2012. Air pollution and health: Bridging the gap from sources to health outcomes: conference summary. *Air Qua. Atmos. Health* 5, 9–62.
- Tartakovsky, D., Broday, D.M., Stern, E., 2013. Evaluation of AERMOD and CALPUFF for predicting ambient concentrations of total suspended particulate matter (TSP) emissions from a quarry in complex terrain. *Environ. Pollut.* 179, 138–145.
- Wu, J., Wilhelm, M., Chung, J., Ritz, B., 2011. Comparing exposure assessment methods for traffic-related air pollution in an adverse pregnancy outcome study. *Environ. Res.* 111, 685–692.